Additive Manufacturing 36 (2020) 101625

Contents lists available at ScienceDirect

Additive Manufacturing

journal homepage: www.elsevier.com/locate/addma

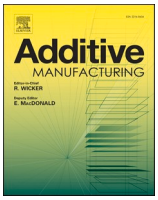

Effects of powder reuse on the microstructure and mechanical behaviour of Al–Mg–Sc–Zr alloy processed by laser powder bed fusion (LPBF)

Laura Cordova [a], Ton Bor [a], Marc de Smit [b], Simone Carmignato [c], Mónica Campos [d], Tiedo Tinga [a]

[a] Department of Mechanics of Solids, Surfaces & Systems (MS3), University of Twente, Drienerlolaan 5, 7522 NB Enschede, Netherlands
[b] Netherlands Aerospace Centre (NLR), Voorsterweg 31, 8316 PR Marknesse, Netherlands
[c] Department of Management and Engineering, University of Padova, Stradella San Nicola 3, 36100 Vicenza, Italy
[d] Department of Materials Science and Engineering, University Carlos III of Madrid, Avda. Universidad, 30, 28911 Leganés, Spain

ARTICLE INFO

Keywords:
Laser powder bed fusion (LPBF)
Powder reuse
Porosity
Scalmalloy®
Al–Mg–Sc–Zr alloy

ABSTRACT

Laser powder-bed fusion (LPBF) technology is one of the additive manufacturing (AM) processes that uses metal powder to produce parts for various industry sectors such as medical, aerospace, automotive and oil & gas. As an 'additive' based process, the material is selectively melted by a focused laser. By this working principle material is added in a layer-by-layer approach only where is needed. Therefore, this technology enables a high reduction of waste by avoiding chips typically generated in 'subtractive' based processes such as milling and drilling. However, to ensure lower waste consumption the metal powder surrounding the solidified part must be reused in subsequent build jobs. Current knowledge on the effect of powder reuse on LPBF builds is mostly limited to titanium- and nickel- based alloys. The aim of this paper is to study the effect of powder reuse on Al–Mg–Sc–Zr, a high strength aluminium-based alloy, manufactured by LPBF. Here, powder properties such as morphology, composition, particle size distribution are studied of virgin (pristine) and reused Al–Mg–Sc–Zr powder. The mechanical properties of specimens made of virgin powder and after four build cycles are analysed and compared to assess the influence of a mixture of virgin and reused powder material on the consolidated material properties. In general, the powder does not present large differences in composition and morphology, only the reused powder presents coarser particle size distribution (PSD) as previously observed in other alloy compositions. The microstructure of the studied specimens is very similar unlike the porosity. The specimens built with reused powder show a few small micro-sized pores which do not show significant differences in the mechanical properties. In fact, the ultimate tensile strength (UTS) and elongation to break of specimens, respectively built with virgin and reused powder are 565 MPa, 13% and 537 MPa, 11%. Based on the obtained results, it is concluded that it is feasible to reuse Al–Mg–Sc–Zr powder in four subsequent build jobs with proper powder sieving and a rejuvenation step mixing 40% of virgin powder.

1. Introduction

Additive manufacturing (AM) processes enable the production of parts with complex features and advanced functionalities that cannot easily be manufactured otherwise [1]. The laser powder bed fusion (LPBF) process employs a high-power laser source to melt metal powder locally and to build up a 3D structure in a layer-by-layer approach. The LPBF process is a highly complex manufacturing process where the material properties depend strongly on the process history. As concluded by Aboulkhair et al. [2], there is a strong relation between the process parameters and the resulting properties of the manufactured part. Laser power, laser speed, particle size distribution, layer thickness, scanning pattern, and temperature of the build plate all have an effect on the thermal history that is key to the development of the microstructure and the mechanical properties, as studied by Amato et al. [3]. Other aspects such as variations in microstructure, porosity, and surface roughness, as discussed by Mower et al. [4], play an important role in the final part performance. The interaction of all influencing factors makes the LPBF process a complex process that is sensitive to small input variations. It explains to a large extent why it has often been difficult to maintain a reproducible process, and unintentional material property and product performance variations are often observed.

E-mail address: l.cordovagonzalez@utwente.nl (L. Cordova).

https://doi.org/10.1016/j.addma.2020.101625
Received 7 June 2020; Received in revised form 21 September 2020; Accepted 23 September 2020
Available online 29 September 2020

After completion of a part by the LPBF process, the part is removed from the build plate. The remaining unused powder on the build plate can in principle be reused for a new build cycle. As concluded by Ardila et al. [5], reusing the powder is key to rendering the LPBF process economically feasible and sustainable as the powder production process is energy and time consuming,. Atomisation processes are often employed to manufacture the powder particles and the typical layer-by-layer approach to building up a part by LPBF requires particles in a narrow size range of 15–80 μm. Particles with dimensions smaller than the lower limit typically show poor flow behaviour when spread over a previously deposited layer. Particles with dimensions above the powder layer thickness, typically between 60 μm and 100 μm for a fused layer thickness of 30 μm and 50 μm respectively, are clearly unwanted as they interfere with the powder spreading process. The powder layer density on the build plate varies as a function of material density, moisture content and powder properties from 30% to 50% as researched in a previous study by the authors [6]. The required limits to the powder size and, in general, to the powder size distribution set constraints on the reuse of powder to safeguard a smooth and reproducible spreading of successive powder layers.

A small portion of the powder may be affected by the heat of the melting process. This may occur when the powder particles were located close enough to a melt pool, yet far enough away not to be included in the part. The amount of powder that is affected depends mainly on the duration of the build cycle, the number of parts and their geometry/size. Often some degree of agglomeration and/or sintering is observed, leading to a few larger particles that sometimes feature satellites and a higher surface roughness. However, an important aspect is spattering of ejected particles from the melt pool that land in the surrounding powder. This usually leads to the formation of agglomerates and oxides that can be found on the powder bed at some distance from the melt pool as studied by Gasper et al. [7,8]. Sieving of the powder intended for reuse is commonly carried out to remove these larger particles and agglomerates formed by sintering and spattering. In this way the maximum size of the powder particles is safeguarded by the sieving mesh dimensions. However, the exposure to heat may also cause other changes to the powder particles and the smaller agglomerates that are within the required dimensional range. Changes in the powder particle shape have been reported to affect the powder spreading process [9], whereas changes in the (surface) chemical composition may modify, for example, the wetting behaviour of the particles. This means that simply sieving out the larger agglomerates and/or sintered powder particles may not be sufficient to maintain a reproducible particle size distribution with predictable behaviour.

The variation of the material properties of LPBF builds due to reuse of powder has been studied before for some metal powders that are often used for LPBF, including titanium, nickel and, to a limited extent, aluminium alloys. The most researched material on reuse behaviour is Ti6Al4V. Some authors have found an increase in the oxygen content after a number of build cycles upon reuse. For example, Quintana et al. [10] detected a rise in the oxygen level from 0.09 wt% to 0.13 wt% after 31 LPBF build cycles. In this case, an increase in the particle size and a moderate increase of the ultimate tensile strength (UTS) were measured as well. The latter was explained by the strengthening effect of oxygen. The plastic elongation at fracture did not show a clear dependency on the oxygen content. Seyda et al. [11] also reported a coarsening effect of the Ti6Al4V powder particles and they observed a decrease in the porosity level during 12 successive build cycles of LPBF. However, the surface roughness of the specimens produced from the reused powder was greater than that of the specimens manufactured from virgin powder. The hardness and UTS of the specimens from the reused powder was also greater than that of the specimens from the virgin powder.

The available literature on reuse of aluminium powders processed by LPBF is very limited and concentrates exclusively on AlSi10Mg, a typical high strength casting alloy. In a recent study, Asgari et al. [12] investigated the microstructure and mechanical properties of AlSi10Mg specimens fabricated by LPBF using virgin and reused powders. The results showed comparable mechanical properties, concluding that reuse is possible for AlSi10Mg powder. Previous studies with a higher number of reuse cycles have also demonstrated the possibility of reusing AlSi10Mg without detrimental consequences to the powder and build properties. Maamoun et al. [13] studied the effect of reusing AlSi10Mg in 18 build cycles. The reused powder of this study, which was sieved in between build cycles using a 70 μm sized mesh, did not show apparent differences in the properties in comparison with the virgin powder, which was also sieved using the same mesh size. The morphology of reused particles was, however, slightly more elongated. A statistical study by Del Re et al. [14] of reusing AlSi10Mg throughout eight build cycles and sieved using a 60 μm sized mesh revealed a systematic decrease of 10 MPa in the yield strength (YS) and UTS and a decrease from 160 to 145 MPa in the high cycle fatigue after eight cycles of reuse. However, reuse did not change the elongation at break and the surface quality of the produced specimens.

Aluminium compositions other than AlSi10Mg have not yet been researched deeply on the aspect of reuse. In previous work of the authors [15], four powders typically used in LPBF (Inconel 718, Ti6Al4V, AlSi10Mg and Scalmalloy) were studied, showing some degree of variation in particle size and morphology after reuse. Powder coarsening due to agglomeration and/or sintering led to an increase in the average particle size and the number of satellites. At the same time, the number of fines (small particles) decreased during continuous reuse, leading to a narrower particle size distribution. The results also revealed that the material with the highest variability to the studied parameters (particle size distribution, morphology, chemical composition and flowability) was AlSi10Mg, despite the low number of reuse cycles (six).

The present work aims to extend the knowledge on the effects of powder reuse for an Al–Mg alloy reinforced with Sc and Zr commercially named Scalmalloy®. This high strength aluminium alloy was developed by APWorks for aerospace applications [16]. There are only a few studies that focus on the characterisation of this material. Spierings et al. [17] studied the mechanical properties achieved after a variety of heat treatments. The maximum hardness and tensile strength of the LPBF printed specimens were obtained after a 4–5 h heat treatment at 325–350 °C. The tensile strength reached values higher than 500 MPa together with a ductile fracture behaviour. These results are similar to values previously reported by Schmidtke et al. [18] under similar processing conditions. In addition, the latter study revealed little or no differences ($< 5\%$) in the static tensile properties when testing specimens built in horizontal and vertical direction in the heat-treated condition.

In the present work, Al–Mg–Sc–Zr specimens employing virgin and reused powder were fabricated by LPBF. A standard heat treatment was applied. The aim of this work is to understand how reuse may impact the static mechanical properties of fabricated flat specimens. A complete characterisation of the builds is carried out by means of porosity and microstructural analysis, hardness measurements and tensile tests. The virgin and reused powders employed to build the specimens were also characterised by morphological analyses and by determination of the chemical composition and particle size distribution.

2. Experimental procedure

2.1. Materials and LPBF process

The Al–Mg–Sc–Zr powder with the composition as listed in Table 1 and supplied by APWorks (Germany) was used in an SLM Solutions machine (Germany) model 280HL to produce 3D printed plates of size 150 mm × 5 mm × 2.5 mm as shown in Fig. 1a. The powder received from the supplier is labelled as ‘virgin’ and the powder that was used at least once before is labelled as ‘reused’. In this case, the powder used to build the ‘reused’ specimens had already been used for four cycles. As the build required a larger amount of powder to reach the height, 40% of

Table 1
Chemical composition (wt%) provided by the powder supplier.

Material	Al	Fe	Mg	Mn	Sc	Si	Ti	V	Zr
Al–Mg–Sc–Zr	Bal.	0.13	4.39	0.49	0.66	< 0.01	0.021	0.013	0.31

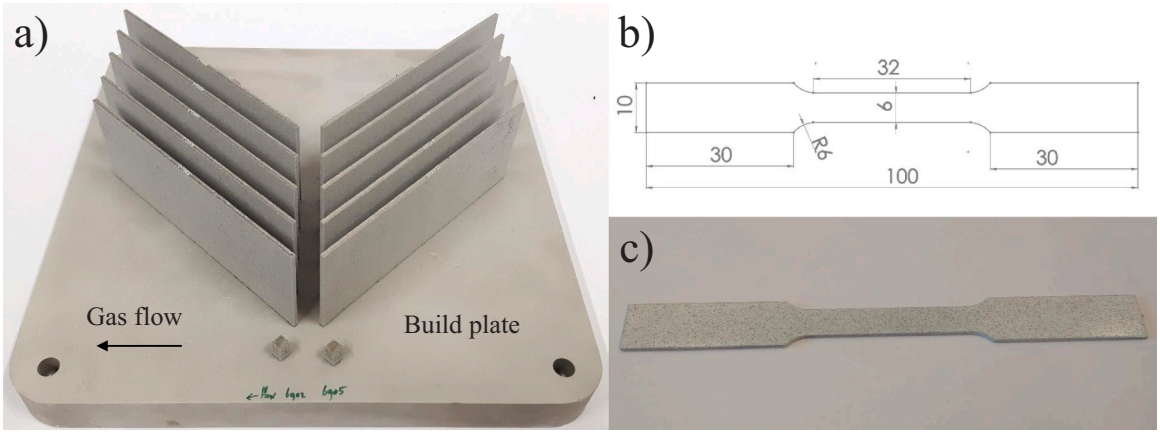

Fig. 1. (a) Beams built by LPBF on the build platform (280 × 280 × 360 mm^3), (b) geometry of the tensile test specimens – dimensions are given in millimetres, 1 mm thickness, (c) the machined and painted tensile specimens.

virgin powder was added to the batch of reused powder, that had not been rejuvenated before, before printing the specimens (rejuvenation). These specimens were thus printed with a mixture of sieved reused powder and virgin powder. Therefore, the sample for characterisation of the reused powder was collected after printing the specimens with a mixture of reused powder containing 60% of the powder after five build cycles and 40% of the powder after one build cycle.

The reused powder is collected from the overflow container and build plate after the LPBF and sieving process. The sieving was performed at the standard PSM100 sieving station from SLM solutions where powder is fed over a sieve which is vibrated, using a combination of low frequency and ultrasonic. The material is sieved under argon. Too large particles which do not pass through the mesh end up at the other end of the sieve and fall in a waste bottle. The sieved-out agglomerates are labelled as 'sieve waste powder'. These agglomerates thus potentially contain powder particles from five consecutive build jobs. Throughout this chapter, the specimens produced from virgin powder are denoted 'virgin powder' specimens, and those from the mixture of reused powder are denoted 'reused powder' specimens.

In order to exclude the role of humidity entrapped in the powder regarding pore formation, an additional build cycle was performed with reused powder (five build cycles) that was vacuum dried before the build job started (cycle 6). Also these manufactured specimens were analysed for the presence of pores.

Process parameters were used to produce the samples with a (laser) volumetric energy density of $E_V = 78$ J/mm^3, using a laser power of 380 W in combination with a scanning speed of 974 mm/s. During the LPBF process, powder layers of 50 μm were deposited to create the 3D structure of solidified material, following a laser scanning pattern with a scan vector rotation of 67°, as proposed by Geiger et al. [19] The build plate was pre-heated to 180 °C. The rest of the parameters were adjusted to obtain the maximum tensile strength and minimum porosity level as shown in a previous study of the authors in which the mechanical properties of AlSi10Mg and Al–Mg–Sc–Zr are analysed and compared [20].

2.2. Post-processing

The produced plates were subjected to a stress relief heat treatment of 1.5 h at 180 °C and a subsequent precipitation hardening treatment of 4 h at 325 °C. In this way, the Al_3 (Sc, Zr) precipitates are formed that give the material its high strength [21].

The surface roughness of the plates was determined using a Keyence Confocal Microscope (VK 9700, Japan) model with a 10× lens. The surface roughness was measured at 16 different locations to determine the average value and relative variation of the surface roughness. A number of printed and machined plates were laser cut to obtain the tensile test specimens following the geometry of the subsize specimen (Fig. 1b) in the ASTM Standard Test Methods for Tension Testing of Metallic Materials (E8/E8M – 15a) [22]. Before the tensile tests, the specimens were sprayed with black and white paint to create a speckle pattern (Fig. 1c) with optimally traceable reference points for Digital Image Correlation (DIC) [23].

2.3. Powder and specimens characterisation

First, the virgin and reused powders were characterised using different techniques. The powder morphology was analysed by scanning electron microscopy using a SEM (FEI Nova NanoSEM 450, Thermo Fisher Scientific, USA) and the chemical composition was obtained by energy-dispersive X-ray spectroscopy (EDX), using an EDX detector (EDAX trident system, AMETEK, Inc., USA) integrated in the SEM. The average values and standard deviation of the chemical composition was obtained from the analysis of 16 particles of virgin powder, 27 particles of reused powder and 28 particles of sieve waste powder. The particle size distribution (PSD) of the powders was analysed by static image analysis using the software Scandium (ResAlta Research Technologies, USA) from the SEM images of the particles. A sample size of at least 4000 particles was used for the analysis. The equivalent mean diameter of the particles was estimated and used to calculate the D10, D50 and D90 values, which are the intercepts for respectively 10%, 50% and 90% of the cumulative particle size distribution. The microstructures of the sieve waste powder and the printed specimens were evaluated using a SEM (FEI Teneo, Thermo Fisher Scientific, USA) integrated with a concentric back scatter (CBS) detector. The digital microscope from Keyence (Japan) of model VHX-5000 was used to study the melt pool regions and the porosity of the specimens printed from both virgin and reused powders. Conventional metallographic preparation procedures were followed. All specimens were etched with Keller's reagent for 20 s to reveal the microstructure.

Table 2
Scanning parameters used for μCT analysis.

Parameter	Value
Voltage [kV]	155
Current [μA]	47
Exposure time [ms]	1420
Nr. of projections	2000
Voxel size [μm]	3

Table 3
Chemical composition (wt%) of virgin, reused and sieve waste powder estimated by EDX.

Element	Virgin	Reused	Waste
Al	93.3 ± 2.1	93.6 ± 2.1	93.4 ± 2.0
Mg	5.2 ± 0.2	5.0 ± 0.2	4.9 ± 0.2
Sc	0.8 ± 0.2	0.8 ± 0.2	0.9 ± 0.2
Mn	0.7 ± 0.3	0.7 ± 0.2	0.6 ± 0.2

Second, the crystal orientation and grain size distribution in the specimens were obtained by employing electron backscatter diffraction (EBSD) and the analysis software AZtecHKL (Oxford Instruments, UK). The specimens and loose reused powder were also analysed by X-ray diffraction (XRD) using the model X′Pert (Philips, The Netherlands) using Bragg Brentano optics with Cu-Kα radiation to identify the phases present in the alloy. The results obtained within the 2θ angle range from 30° to 90° were processed using the X′Pert HighScore program. The microstructural analysis, XRD measurements, porosity measurements and hardness tests were done along the width of the machined plates.

Third, the porosity is studied by two different techniques: optical microscopy and 3D μCT. These techniques are complementary for porosity analysis. Micro-computed tomography (μCT) was used in this work to analyse porosity in a non-destructive way, obtaining high-resolution and accurate three-dimensional reconstructions of the samples [24]. A volume of 5 mm × 5 mm × 1 mm of the printed specimens was analysed using a metrological μCT system (Nikon X-Tek MCT225, Nikon Metrology/X-Tek Systems Ltd., UK), equipped with a 225 kV micro-focus X-ray source and a flat panel detector with 2000 × 2000 pixels (16 bit), and located in a temperature-controlled cabinet. Two samples of each type of powder where analysed to calculate the average and standard deviation.The selected scanning parameters are listed in Table 2. The power of the μCT scan was kept below 7 watts in order to maximise the metrological structural resolution of the scan results [25] Dimensional evaluations and analyses of internal defects were conducted using the analysis and visualisation software VGStudio MAX 3.2 (Volume Graphics GmbH, Germany) and implementing a dedicated procedure for traceable porosity measurements [26].

Fourth, an automatic micro indentation testing system (LECO AMH 43, LECO Corporation, USA) was used to compare the Vickers hardness (HV) values of the plates built with virgin and reused powder. Five indentations along the width of the machined plates were analysed, following the ASTM Standard Test Method for Vickers Hardness of Metallic Materials (E 92 – 82). The samples taken from the machined plates were embedded in epoxy resin and polished to a 'mirror-like' surface before the indentations were applied using a load of 3 N. The mechanical properties were studied using tensile testing with a specimen geometry as shown in Fig. 1b. The specimens were tested with a Zwick/Roell tensile test machine equipped with a 5 kN load cell and a strain rate of 0.001 s^{-1}. At least five specimens of each type of powder were tested with a cross-section of 6 mm^2 as shown in Fig. 1. A camera captured live images of the test specimens for the strain analysis. The latter was done using the evaluation software for 3D testing (GOM correlate, Germany) a digital image correlation (DIC) software program for materials research and component testing, by using a virtual extensometer length of 20 mm.

Finally, after the tensile tests, the fracture surfaces of the specimens were studied with a SEM (Jeol JSM-7200F, Japan), facilitating the understanding of the fracture behaviour of the materials. The specimens were glued to a holder for SEM examination in the vertical direction, exposing the fracture surface.

3. Results

3.1. Powder characterisation

The virgin and reused powders are sieved and analysed. The sieve waste powder remaining after sieving is analysed as well. The next four subsections present the results for the morphology, the composition, the PSD and the sieve waste powder microstructure, respectively.

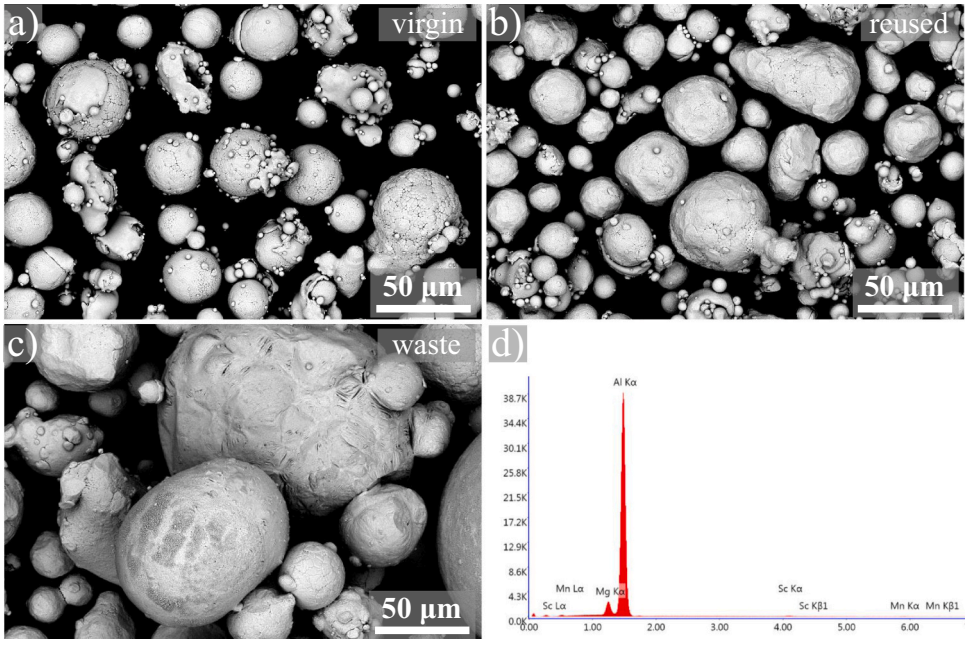

Fig. 2. SEM images of the (a) virgin powder, (b) reused powder and (c) powder collected from the sieve waste. (d) X-ray peaks used for analysis of constituent elements.

Table 4
Particle size values (μm) for three diameter distribution subsets as obtained by image analysis.

Diameter	Virgin	Reused	Waste
D10	4.15	5.65	14.50
D50	21.50	26.55	30.45
D90	45.40	50.70	54.10

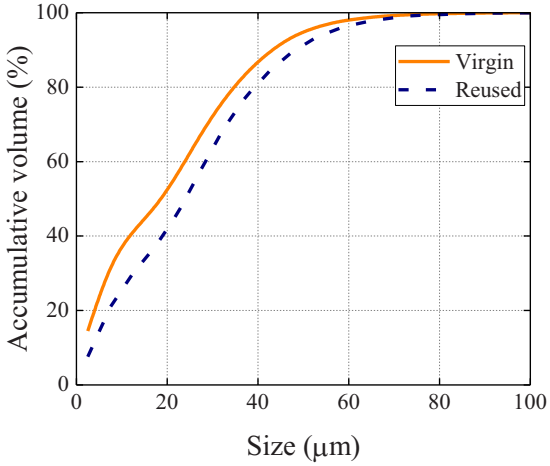

Fig. 3. Particle size distribution of virgin and reused powders.

3.1.1. Powder morphology

The morphologies of the virgin powder, the reused powder and the sieve waste powder are shown in Fig. 2. The images show a relatively irregular powder morphology where the larger powder particles often have many small satellites attached. Although there are no large differences between the virgin and reused powder, the reused powder does show fewer satellites. The sieve waste powder also contains larger agglomerates (Fig. 2c) produced from sintering of small spherical particles and from spattering during five consecutive build cycles. It is important to remove these relatively large and unregularly formed agglomerates to prevent problematic spreading behaviour during subsequent build jobs with reused powder. This also holds to some degree for the small satellites visible on and attached to the virgin and reused powder particles in Fig. 2a and b. This may result in a lower surface quality of the final LPBF part. The observed sieved-out agglomerates in Fig. 2c are usually larger than 100 μm, which is the mesh size of the sieve used to condition the reused powder.

A further analysis of the sieve waste shows that not only agglomerated particles larger than the mesh size are present, but also non-agglomerated particles with dimensions down to the smallest value available, see Fig. 2c. Apparently, the sieving process is not very efficient as loose fine particles are included in the sieve waste.

3.1.2. Powder composition

An EDX semi-quantitative analysis (Fig. 2d) has been carried out to estimate the composition of the virgin powder, reused powder and the sieve waste powder. The values in weight percentage and standard deviation for each of the main elements are shown in Table 3. There are no significant differences in chemical composition between the virgin, reused and sieve waste powder. Some sieve waste particles contaminated with a high amount of oxygen were found in the reused powder and the sieve waste powder. However, this EDX measurement is not suitable for determining the exact amount of trace elements such as oxygen.

3.1.3. Particle size distribution (PSD)

The PSDs were obtained from analysing particles in SEM pictures of the virgin, reused and sieve waste powder and determining equivalent diameters for each particle (see Section 2.3). The results are shown in Table 4 and represented in Fig. 3. The parameters extracted from the PSD curves, such as D10, D50 and D90 (i.e. the maximum size of the lower 10%, 50% (= average size) and 90% of the particles, respectively) show a slight change towards larger particle size when comparing the reused powder to the virgin powder. This suggests that the relative contribution of smaller particles in the PSD of the reused powder has fallen below that of the virgin powder.

Another interesting observation is the set of parameters extracted for the sieve waste powder. The values of D10, D50 and D90 are all smaller than the mesh size opening of 100 μm, clearly indicating that also (large amounts of) powder with dimensions smaller than the sieve mesh opening is part of the sieve waste. This is surprising, as the mesh size opening is in principle large enough for the powder to pass. These results are in line with the SEM pictures shown in Fig. 2c, where a large number of relatively small particles, i.e. smaller than the mesh opening of 100 μm, were observed.

3.1.4. Microstructure of a particle agglomerate from the sieve waste powder

A closer look to the cross-section of an agglomerate particle from the sieve waste powder is shown in Fig. 4. Such an agglomerate is most probably the result of spattering that occurred during the laser scanning and melting of the metal powder. Fig. 4b shows the interface between the original particle and the molten material, where the boundary of the original particle is indicated by arrows. As a result of an incomplete bonding and due to the high-speed solidification, fine pores appear at the interface.

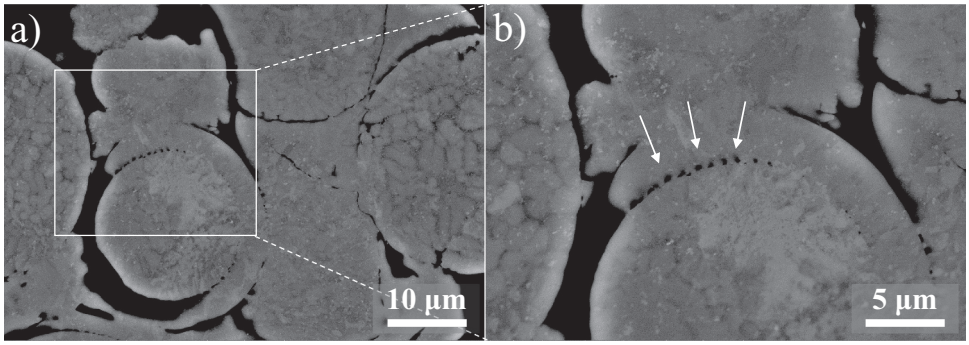

Fig. 4. SEM images at (a) low and (b) high magnifications of the cross-section of particles collected from the sieve waste powder after five reuse cycles. The arrows indicate the intersection of two particles bonded together.

Table 5
Average surface roughness, *Ra* of virgin, reused and machined specimens.

Specimen	*Ra* (μm)
Virgin	28.6 ± 3.8
Reused	30.7 ± 3.3
Machined	3.6 ± 0.2

Table 6
Porosity, sphericity, average and maximum pore size of 'virgin powder' specimens and 'reused powder' specimens.

Powder condition	Porosity (%)	Average Sphericity	Average pore size (μm)	Maximum pore size (μm)
Virgin	0.06 ± 0.01	0.56 ± 0.05	17.8 ± 7.7	108.1
Reused	0.15 ± 0.01	0.61 ± 0.04	16.7 ± 6.5	126

3.2. Specimen characterisation

3.2.1. Surface roughness

The average surface roughness (*Ra*) of the as-built specimens is shown in Table 5 for specimens built with virgin and reused powders. The relatively high surface roughness values are usually detrimental to the mechanical properties of the produced material due to local stress concentrations facilitating crack growth and fracture. Hence, the surfaces of both sides of the plate were machined down to a final specimen thickness of 1 mm, which strongly reduced the average surface roughness, as also shown in Table 5.

Fig. 5a and b show the 3D profile of the surface roughness (also obtained with the Confocal Microscope) of the specimens produced with virgin and reused powder. The differences found in the plate surfaces, as also shown by the average roughness values *Ra* in Table 5, are within the range of the standard deviations obtained from the measurements. On the other hand, the machined specimens (Fig. 5c) show a much smoother surface as more than 0.5 mm of material was removed on each side of the plates. The mechanical testing and further characterisation of the printed parts of this work were carried out on the machined specimens alone.

3.2.2. Microstructure

The optical microscopy images of the cross-sections of the melt pools present in the 'virgin powder' specimens and the 'reused powder' specimens are shown in Fig. 6. This clearly reveals a pattern of stacked weld pools, caused by the printing pattern that was followed during the LPBF process. The darker areas that form the melt pool (MP) boundaries

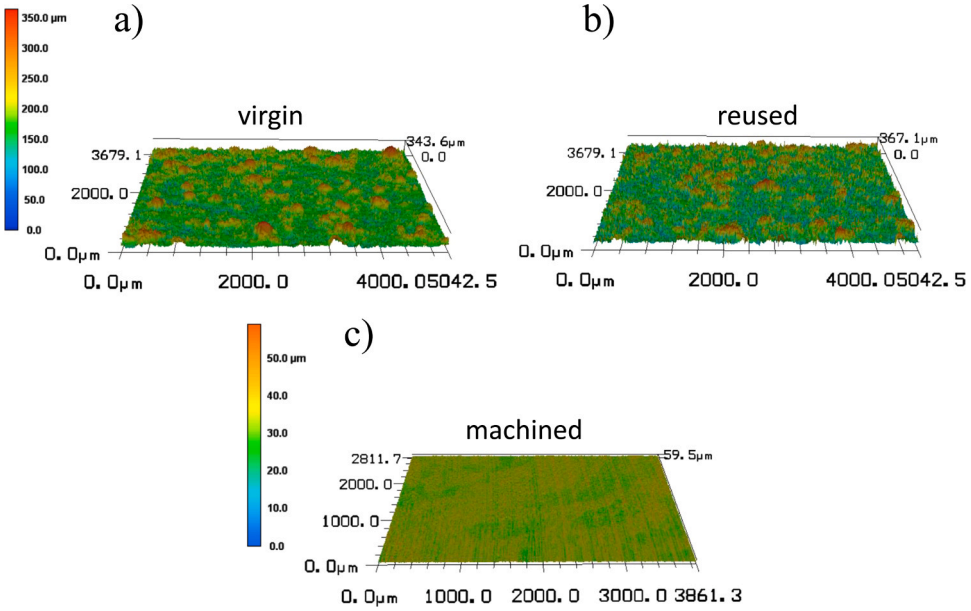

Fig. 5. 3D surface profile of specimens: (a) as-built from virgin powder, (b) as-built from reused powder and (c) after machining.

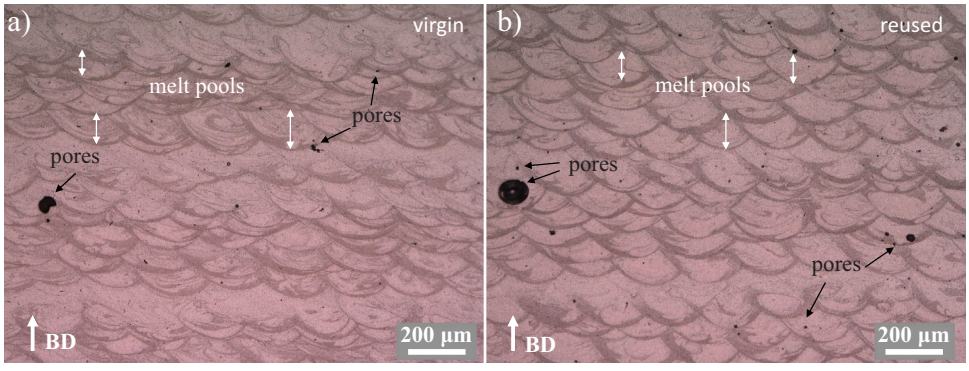

Fig. 6. Optical image of the microstructure of specimens from (a) virgin and (b) reused powder. BD indicates the building direction.

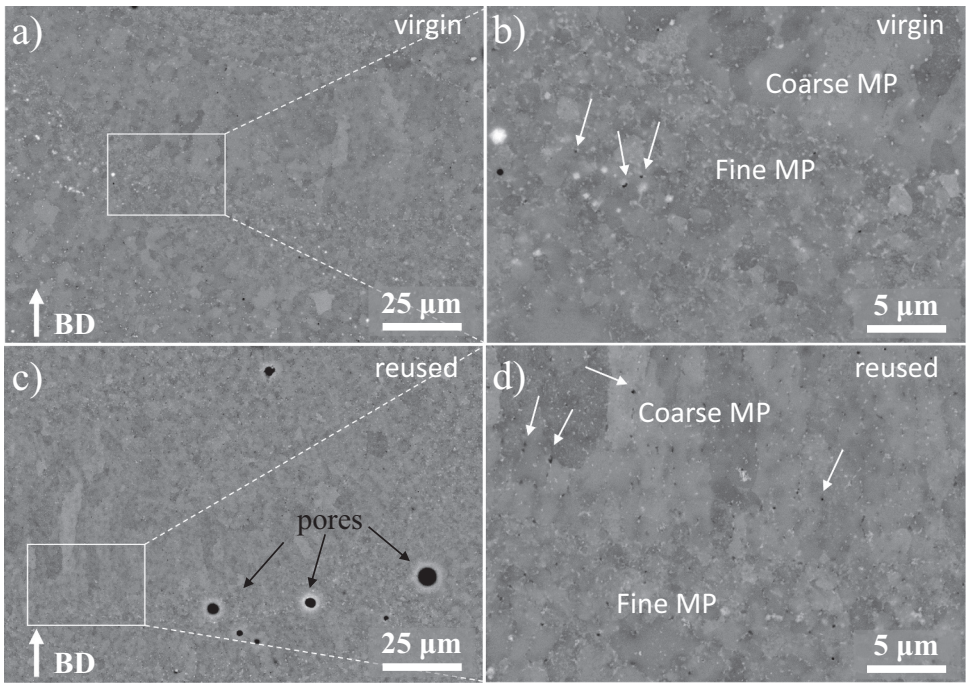

Fig. 7. SEM images of the microstructure of specimens built with virgin powder at (a) low and (b) high magnifications. Specimens built with reused powder at (c) low and (d) high magnifications. Black arrows indicate pores developed in the specimens built with reused powder. White arrows indicate nano-scale pores.

consist of fine grains that surround the elongated grains which typically grow in the direction of heat dissipation. This holds for the specimens made from both the virgin and the reused powders. The melt pools of the reused specimen seem larger and more repeatable (periodic) than those of the virgin specimen. Additionally, the virgin specimen shows a larger area of fine grains in which the melt pool boundaries are less clearly visible. This may be related to sample preparation.

The boundaries of the melt pools observed in Fig. 6 are composed of fine grains, which were formed as the result of rapid solidification and presence of precipitates in the melt. The precipitates can act as seed crystals and consequently become intergranular. More detail on the microstructure is shown for a virgin and a reused specimen in Fig. 7b and d respectively. The difference between these boundary regions and the coarser MP regions is characterised by the larger and more elongated grains as well as the bright white coloured particles at/between the grain boundaries of the fine grains. These particles have the characteristics of the Al_3(Sc, Zr) precipitates previously reported by Spierings et al. [27]. In addition, grain boundary particles of various compositions (Al–Mg-oxides) were observed, these contribute to the very fine-grained bi-modal microstructure characteristic from the LPBF process.

Nanometre-scale pores (indicated by white arrows) are also observed between the grains, which might be hydrogen porosity. The porosity observed in Fig. 7c consists of relatively large spherical pores with a diameter up to ~ 100 µm, as previously observed in Fig. 7b. They probably formed due to gas bubble entrapment in the melt pool just before (rapid) solidification [28].

The EBSD maps in Fig. 8a and b show the grain orientations and size distribution. Both the zones with relatively fine grains and those with larger grains are clearly visible, in line with the results of the optical analysis of Fig. 6a and b. No clearly discernible texture is apparent from both the 'virgin powder' specimens and 'reused powder' specimens, as the grain orientations (as indicated by the different colours) seem to be distributed randomly. The grain size distributions obtained from the EBSD maps show no significant differences either, as is shown in Fig. 8c. In fact, the average grain sizes for 'virgin powder' specimens and 'reused powder' specimens are very similar, 2.3 µm and 2.4 µm, respectively. Therefore, it is concluded that potential differences in the mechanical properties cannot be due to variations in grain size, and thus should be attributed to PSD changes, and its effect on the processing window.

3.2.3. *Phase analysis*

The XRD spectra of reused powder, as well as those of the virgin and reused LPBF specimens (Fig. 9a), reveal diffraction peaks[1] [29] corresponding to the same phases, α-Al and Al_3(Sc, Zr), within the 2θ range of 30–90°. The ratios of intensities among the various {*hkl*} peaks observed in this work are not much different from those of an isotropic sample [30], again indicating the absence of strong textural components. In other studies the relative intensity of the Al {200} Bragg peak is often significantly enhanced pointing at a texture with a <100> direction perpendicular to the sample surface [31,32]. An unexpected observation is the shift of the XRD pattern of the reused specimen with respect to the patterns of the virgin specimen and reused powder sample. This becomes clear from Fig. 9b and c, which show the details of the {111} and {200} shift reflections, respectively. The curves in Fig. 9b and c do not show the real intensity therefore the shape of the curves appear distorted. There may be various sample-related reasons for the shift of a diffraction peak, including the presence of residual stresses, changes in the chemical composition and changes in microstructural constitution (presence/absence of precipitates) [33]. It is not immediately clear what the origin of the peak shift is in this case. The microstructures of the virgin and reused LPBF samples are similar and both samples have undergone the same post-processing heat treatment. However, the reused powder had a different thermal history than the virgin powder, which may have affected the lattice parameters of the printed samples.

3.2.4. *Porosity studied by optical microscopy and 3D µCT*

The values of the porosity level, pore sphericity (defined as the ratio between the surface of a sphere with the same volume as the pore and

[1] Note that each {*hkl*} diffraction peak in the diffractogram is composed of a Kα1/Kα2 doublet, where the Kα2 peak is shifted to higher diffraction angles and typically has an intensity that is about half of that of the Kα1 peak.

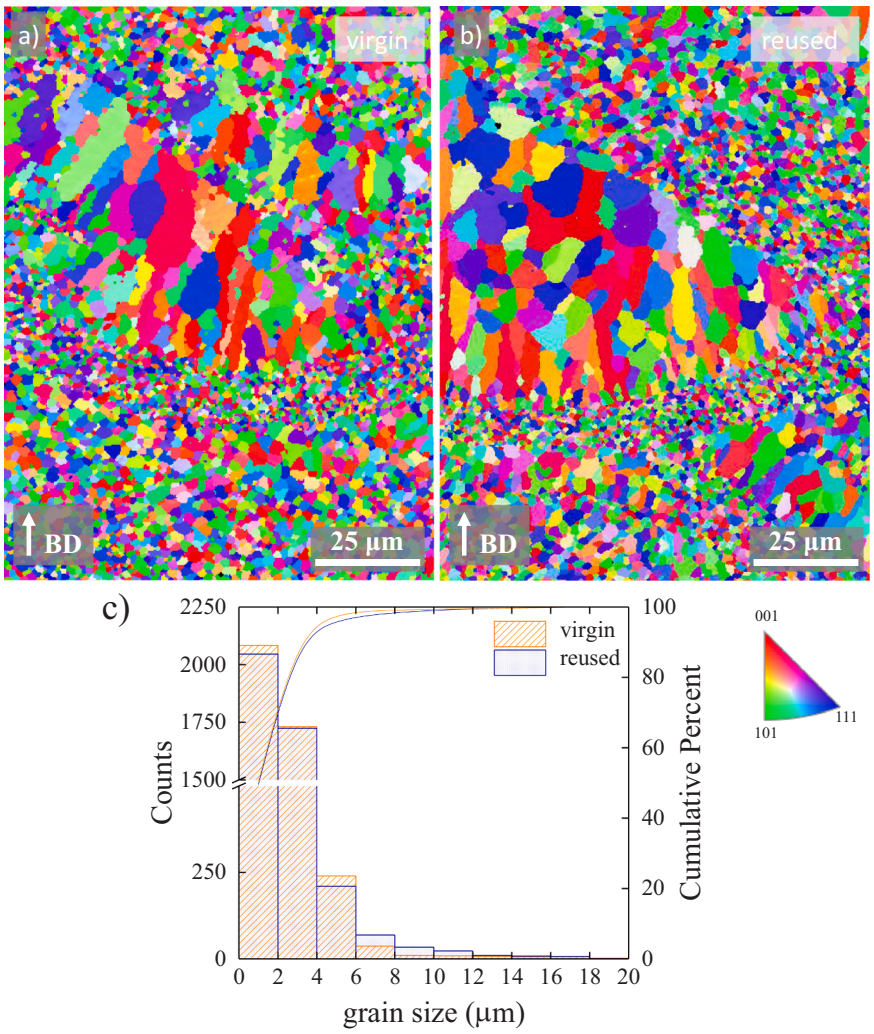

Fig. 8. EBSD maps of the grain orientation of (a) 'virgin powder' specimens and (b) 'reused powder' specimens. (c) Histogram of the grain size distribution: the bars (and left axis) represent the grain counts, the line (and right axis) shows the number based cumulative distribution.

the surface of the pore), average and maximum pore size were determined by 3D µCT, see Table 6. The porosity levels in the 'reused powder' specimens (0.15%) are almost three times higher than in the 'virgin powder' specimens (0.06%). The other quantities set out in Table 6, such as the sphericity and pore size, do not show significant differences between virgin and 'reused powder' specimens. The maximum pore size of the reused specimen is slightly larger than that of the virgin specimen for these samples.

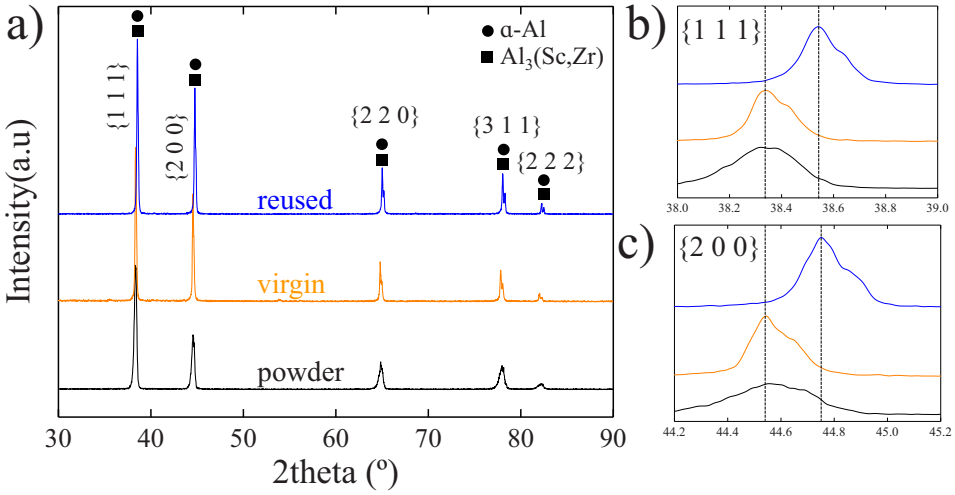

Fig. 9. (a) XRD diffractograms of specimens built from reused and virgin powder, and reused powder. Details of the peaks: (b) {111} and (c) {200}.

As mentioned in the experimental section, porosity analysis was also performed in a third experiment with reused powder previously vacuum dried overnight. The number of pores detected in these specimens was not different from that of the reused samples that were processed without the additional vacuum drying step.

The optical micrographs of Fig. 10a and b show the pores on a polished cross-section of specimens built from virgin and reused powder respectively. The pores are distributed homogenously over the area in both cases and have a mostly spherical shape, as was observed before in Section 3.2.1. It seems that the 'reused powder' specimens show a higher number of evenly distributed micro-pores than the 'virgin powder' specimens. In fact, this is confirmed by Fig. 10c and d where the 3D μCT scanned volumes (5 mm × 5 mm × 1 mm) of the virgin and 'reused powder' specimens are shown. The volume of each pore is represented by the coloured scale on the left of each image. This reveals that the largest pores in the 'reused powder' specimens have a larger volume than those in the 'virgin powder' specimens, as can be derived from the maximum value of the volume bar scales in Fig. 10c and d.

More details on the volume of each pore and the diameter distribution are shown in Fig. 11a, which was obtained from the μCT analyses. Even though the pore distributions do not appear to differ much between the 'virgin powder' specimens and 'reused powder' specimens, the latter shows significantly more small pores (with a diameter up to 60 μm) than the virgin specimen, as is shown in Fig. 10b. In Fig. 11a also some data points of pores with relatively large diameters and small volumes can be found, which correspond to rather elongated pores with a low sphericity index.

The pores were divided into four groups according to their volume: group (I) – pores smaller than 1×10^{-5} mm^3, group (II) – pores between 1×10^{-5} mm^3 and 5×10^{-5} mm^3, group (III) – pores between 5×10^{-5} mm^3 and 1×10^{-4} mm^3 and group (IV) – pores larger than 1×10^{-4} mm^3. For each group the total volume of the pores and the number of pores in that group was calculated, as shown in Fig. 12. This plot reveals large differences in porosity distribution between the 'virgin powder' specimens and 'reused powder' specimens, especially for groups I and II. In the case of groups III and IV (the largest pores), the number of pores and volume are similar. Note that the number of large pores (group IV) in 'reused powder' specimens is lower than in the 'virgin powder' specimens specimen, but the total volume of the group is nevertheless higher. This means that the large pores (group IV) in the 'reused powder' specimens are on average larger than in the 'virgin powder' case.

3.2.5. Mechanical properties

Typical engineering stress-strain curves of the 'virgin powder' specimens and 'reused powder' specimens as obtained from tensile tests are shown in Fig. 13. The test results show the typical serrated yielding behaviour of Al–Mg alloys related to the Portevin–Le Chatellier effect, as previously observed by Spierings et al. [17]. In this study a maximum local strain of ~ 24% was measured by DIC, although the (global) elongation at break is considerably lower (~ 12%), as observed in Fig. 13. Given the large elongations obtained in tensile tests it is concluded that Al–Mg–Sc–Zr alloy under static loads shows a highly ductile behaviour for both 'virgin powder' specimens and 'reused powder' specimens.

An overview of the mechanical properties of the LPBF specimens produced with virgin and reused powder is shown in Table 7, together with data from literature for similar processing and post-processing conditions. The hardness values obtained are in between the values found in the literature for the same material built with virgin powder and given similar heat treatments. The hardness of the specimens built with reused powder tends to have lower values than for the specimens built with virgin powder. This slight drop is also observed for the UTS, YS and elongation at fracture. However, most of the differences between 'virgin powder' specimens and 'reused powder' specimens are not significant in magnitude. After comparing the static tensile properties, it can be concluded that in general the results obtained with the printed 'virgin powder' specimens and 'reused powder' specimens are comparable to existing literature of this alloy.

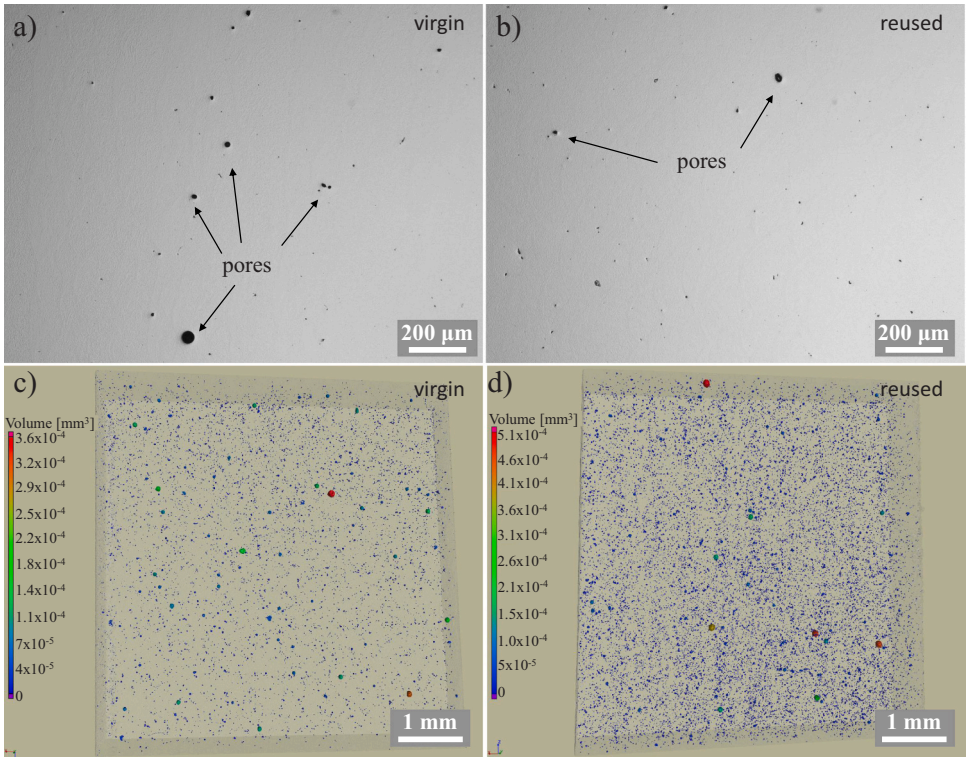

Fig. 10. Optical micrographs of the porosity at a cross-section of: (a) 'virgin powder' specimens and (b) 'reused powder' specimens. 3D μCT reconstructions of a 5 mm × 5 mm × 1 mm volume of: (c) 'virgin powder' specimens and (d) 'reused powder' specimens.

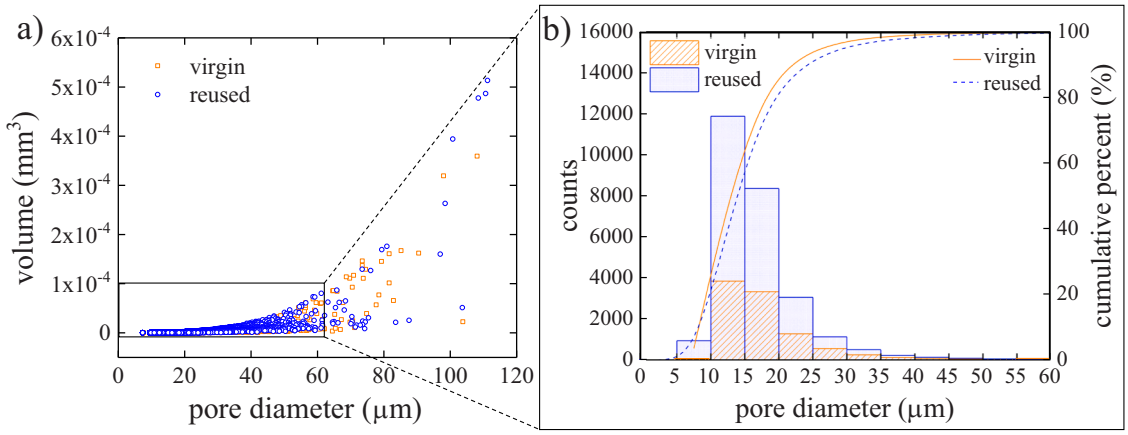

Fig. 11. (a) Relation between pore diameter and volume (b) Detail of the pore distributions up to 60 μm. Bars (and left vertical axis) for the pore counts, line (and right axis) for the cumulative distribution.

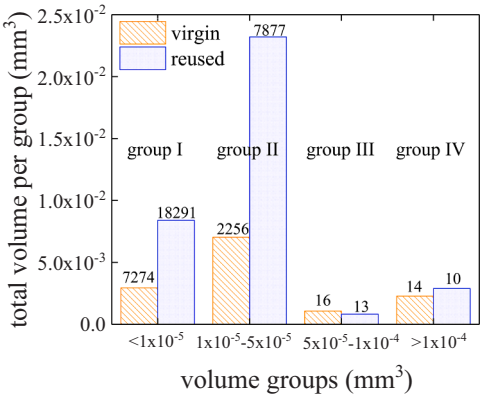

Fig. 12. Total pore volume for four size-groups of pores, for the 'virgin powder' specimens and 'reused powder' specimens (left vertical axis). Each bar has a label indicating the number of pores belonging to that group.

3.2.6. *Fractography*

The presence of pores, in combination with the ductility of the material, determines the fracture behaviour and fracture surfaces. Fig. 14 shows images at low and high magnification of the fracture surfaces of the specimens built with virgin and reused powder after the tensile tests. The micro-pores previously observed by μCT are also present in the fracture surfaces, as shown in Fig. 14a and c. The number of these pores is higher in the 'reused powder' specimens. Both materials show fracture surfaces covered by dimples of a size smaller than 2 μm (Fig. 14b and d), indicating a high degree of local plastic deformation and ductility. Small particles can be observed in the middle of the dimples of Fig. 14b and d, as shown by the detailed micrographs and indicated by dashed arrows. These are most probably the strengthening Al_3–(Sc,Zr) precipitates, usually sized 50–100 nm [34], originating from the precipitation hardening heat treatment that was given to both the 'virgin powder' specimens and 'reused powder' specimens. These precipitates have a relatively high strength, which prevents them from plastically deforming. During the final stages of the tensile test, when the hydrostatic component of the local stress field becomes larger in the necking region, the precipitates get detached from the surrounding matrix. The matrix strongly deforms, forming the dimples, but the small micro cracks around the particles grow out, leading to fracture of the sample [35].

4. Discussion

In the previous sections a detailed comparison and characterisation of virgin and reused powder, as well as samples manufactured from these powders by LPBF, has been performed. The powder morphology and chemical compositions are virtually the same for virgin and reused powder. The analysis of the particle size distributions revealed that the contribution of particles with a relatively small size is smaller for reused powders. Apparently, some of the finer powder particles are systematically removed during sieving after subsequent build cycles. Possible reasons include the very complex handling of the polydisperse powder that may induce unwanted separation effects, leading to less homogeneous powder mixtures [36]. This is often observed in separation methods of large batches of fine and low-density powders, which tend to agglomerate. The smaller particles are also more easily incorporated in agglomerates that develop in the heat affected zones next to the melting zones [37–39], see for example the agglomerates in Fig. 2c and the SEM image shown in Fig. 4. Some of the smaller particles were extracted by the sieving process: they appear in the powder sieve waste, even though these particles have dimensions much smaller than the sieve mesh size (see Fig. 2c). The rejuvenation step, where virgin powder was added to the sieved reused powder of the last build cycle, restored the PSD of this powder to some extent.

The characterisation of the samples manufactured by LPBF with the virgin and reused powder revealed no big differences in the microstructures and phases present. The shape and size of the melt pools (Figs. 6 and 7), the grain size and size distributions (Fig. 8) are all very similar and this also holds for the crystallographic phases that appear after manufacturing and dedicated precipitation heat treatments (Fig. 9). This is, of course, no surprise given the fact that only the PSDs

Table 7
Mechanical properties for LPBF-Al–Mg–Sc–Zr from literature and current research.

Machine	Condition	HV	UTS (MPa)	YS (MPa)	ε (%)	Source
SLM Solutions 280HL	325 °C/4 h (virgin)	161 ± 2	565 ± 14	447 ± 6	13 ± 1	Current work
SLM Solutions 280HL	325 °C/4 h (reused)	157 ± 3	537 ± 6	443 ± 6	11 ± 1	Current work
EOS M 270	325 °C/4 h	177	530	520	14	Schmidtke et al. [18]
ConceptLaser M2	325–350 °C/4 h	137[a]	530 ± 12	453 ± 20	9.5	Spierings et al. [17]

[a] The hardness value was converted from 135HB for comparison.

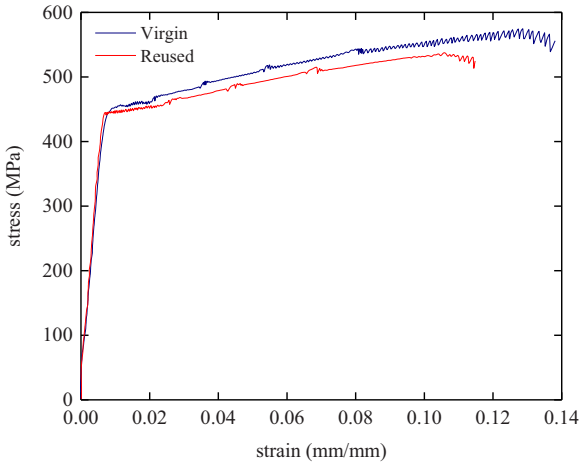

Fig. 13. Typical engineering stress-strain curves of 'virgin powder' specimens and 'reused powder' specimens.

show minor differences at the lower side and the chemical composition of reused powder has not changed after various build cycles.

The porosity levels of the manufactured samples as determined by 3D μCT are relatively low, with values of 0.15% or lower, but it is interesting to see that the value for the specimens made with the virgin powder is clearly lower than that of the reused powder: 0.06% versus 0.15%. Further analysis of the number of pores, their shape and their volume showed that the average pore size and the pore sphericity are similar, but the number of pores with a diameter between 10 μm and 30 μm is substantially higher for the samples manufactured with reused powder (see Table 6 and Figs. 10 and 11). The total number of pores observed in a volume of 25 mm^3 is of the order of 25,000 and 10,000 for the analysed reused and virgin samples, respectively. This corresponds to average numbers of pores of 1000 and 400 per mm^3. The pores are relatively small and, despite their high number, they should not have a significant effect on the mechanical behaviour, given the fracture toughness of this type of alloy. This is also reflected in the mechanical and fracture properties of the tested tensile specimens, as they do not show large differences between the samples manufactured from virgin and reused powder. The hardness and tensile test results are in very good agreement with those in previous studies on this material with similar processing conditions. In addition, the material proved to have a highly ductile fracture behaviour, independent of the powder employed, instead of a catastrophic brittle fracture more typically observed in porous structures. In general, a higher porosity level in the material enhances damage mechanisms like fatigue and creep. Fatigue cracks could more easily initiate at pores, thus reducing the fatigue life. Similarly, void formation during a creep process is also enhanced by the presence of pores [40].

It is well known that even under optimal process conditions the formation of pores during the LPBF process cannot always be prevented [41]. The presence of the larger number of voids in the samples manufactured from reused powder may be ascribed to the reduced number of small particles. The small powder particles are often added to fill up the space between the large particles and increase the packing density [42]. A better packing density during the spreading process also decreases the amount of open space between the stacked powder particles. During the melting stage the powder particles have to melt and coagulate to form a pore free melt pool that subsequently solidifies. However, the typical high-speed conditions of laser heating and subsequent cooling may cause the formation of pores [43] and it seems reasonable to assume that the chances of pore formation are higher when the stacking density is reduced [44]. The presence of a larger amount of inter-particle space for the reused powder is also illustrated in Fig. 15.

In the presence of humidity, pore formation is enhanced through the decomposition of water molecules. The additional build cycle performed with vacuum dried powder did not show clear differences from that of the reused samples that were processed without the additional drying step. In other words, the results of the reused samples presented in this

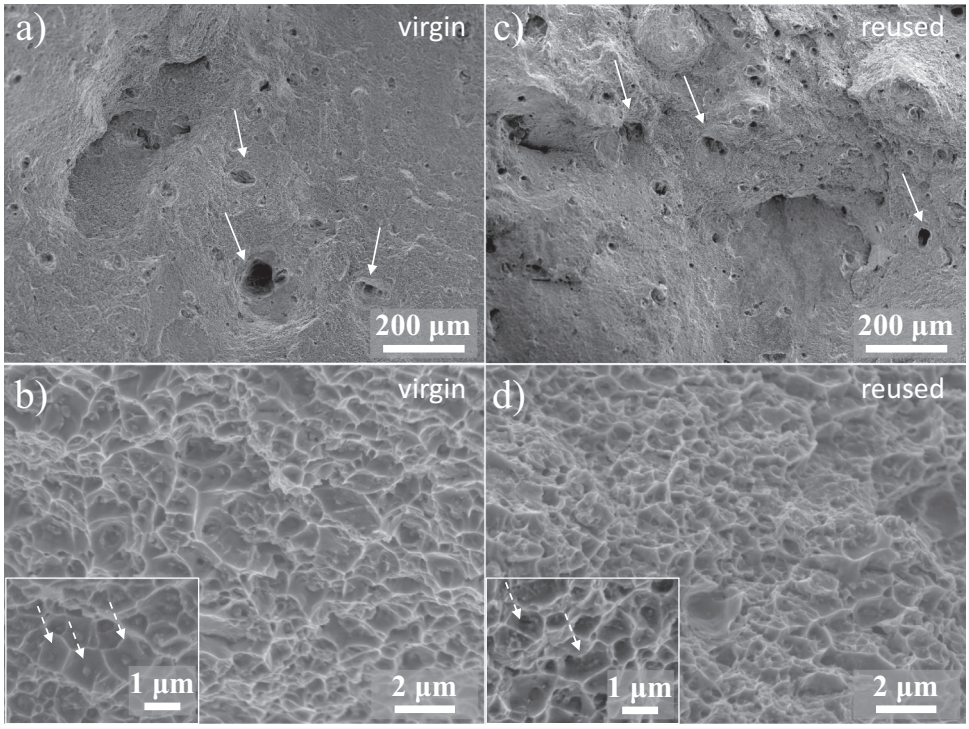

Fig. 14. SEM images of the fracture surfaces of the tensile specimens: (a) and (b) virgin low and high magnification; (c) and (d) reused low and high magnification.

work have not been affected by the (possible) presence of moisture present in the powder batch and/or build chamber.

Further analysis of the results of the tensile tests has shown that the onset of necking occurs at slightly higher values of the engineering strain for 'virgin powder' specimens than for 'reused powder' specimens: 12.5–11.5%, respectively. As the strain hardening behaviour of the tensile test specimens is quite similar, independent of the type of powder, the larger engineering strain at the onset of necking explains the slightly higher value of the tensile strength of the virgin powder based tensile test specimens, see also Table 7. Disregarding the presence of the Portevin–le Chatellier effect, it is tempting to relate this effect to the higher density of micro-sized pores present in the reused samples, which possibly promotes an earlier necking effect. In fact, after the onset of necking, a series of events typically occurs that lead to fracture of a tensile test specimen. This process starts with the initiation of micro voids on inclusions/precipitates, followed by void growth, void coalescence and fracture [45]. However, a large number of micro voids (10–30 μm) are already present in the current LPBF specimens (see Fig. 11b) and these could locally accelerate the initiation stage of void formation around the strengthening precipitates (visible in Fig. 14b and d). Possibly, this may even initiate the start of the necking stage. The presence of a large number of these micro voids in the fracture surfaces supports this hypothesis, see Fig. 14a and c. It may also explain why the reused samples are more sensitive to this effect than the virgin samples, as the number of micro voids is larger for the reused samples.

The relatively small differences between the microstructure and mechanical/fracture properties of virgin and reused Al–Mg–Sc–Zr powder indicates that there are no insurmountable obstacles for the reuse of Al–Mg–Sc–Zr (under the conditions tested in this work). Sieving of the powder after a build is important to prevent incorporation of agglomerates/spatter from previous production steps, which could impair powder spreading in subsequent builds. Rejuvenation has been included in the powder handling between successive build jobs to prevent excessively large changes in the particle size distributions from one build job to another. This seems to have worked properly as well. So, no special precautions other than normal powder handling strategies, including proper rejuvenation, are required for reuse of Al–Mg–Sc–Zr powder for LPBF based AM.

On the other hand, it is worth noting that the number of reuse cycles (four) is relatively low when compared to industrial use, where powder is reused higher number of cycles. Usually virgin powder is added to ensure the minimum quantity for a specific build height. In this case, particles of previous build jobs would mix with new powder. The effect on un-regulated mix of powder of different qualities might need additional insight.

Future work may concentrate on understanding and improving the sieving process: apparently, not only the relatively large powder particles with a size larger than the mesh opening diameter were sieved out, which could be considered logical, but powder particles with smaller dimensions were collected in the sieve waste as well. This should be avoided.

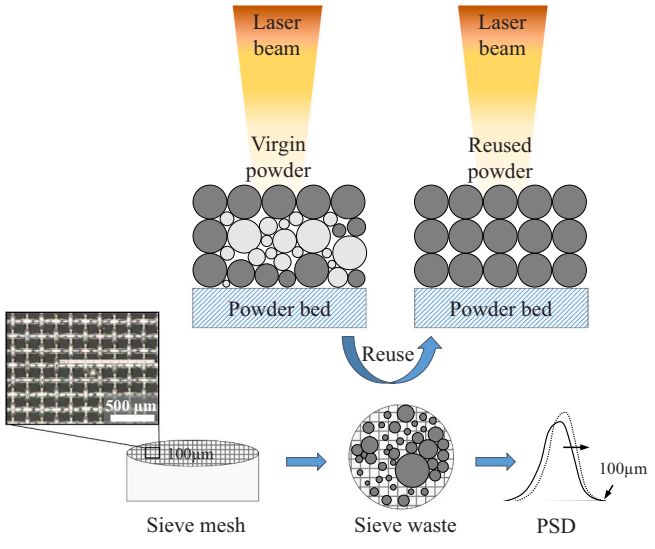

Fig. 15. Reusing cycle of LPBF metal powders: virgin powder is melted to create a printed part, the remaining powder is sieved and loaded again into the LPBF machine. This causes narrowing of the PSD and therefore a lower packing density.

5. Conclusions

In this study, the properties of parts built by LPBF with virgin and reused Al–Mg–Sc–Zr powder were investigated. The particles of virgin powder, reused powder and sieve waste powder were examined. The reused powder was collected after four subsequent build jobs including a rejuvenation step with 40% virgin powder. The morphology, PSD, chemical composition and microstructure were compared. In addition, the microstructure, porosity and mechanical properties of LPBF parts built out of virgin and reused powder were determined. Both powders and LPBF parts exhibited similar properties when comparing the virgin and reused parts produced. Based on the experimental results presented and discussed in this chapter, the following conclusions are drawn:

1. The chemical composition of the virgin powder, reused powder and sieve waste powder is very similar. Only a small contamination with oxygen was found in a few particles of the sieve waste powder.
2. The mean particle size of the reused powder is slightly larger than that of the virgin powder. The sieve waste contains considerable amounts of large particles (as it should), but also fractions of particles with a size smaller than the sieve mesh size.
3. The microstructure of the specimens built with virgin powder is very similar to the specimens built with reused powder.
4. The porosity levels in the 'reused powder' specimens are three times higher than in the 'virgin powder' specimens, but are particularly concentrated in a larger number of small micro-sized pores.
5. Parts made from virgin and reused powder show a comparable strength and both have a ductile fracture behaviour.
6. The observed changes in the particle size distributions due to reuse and sieving could be related to the number of small micro-sized pores (10–30 μm) in the specimens built with reused powder. This did not lead to significant differences in the mechanical properties.

Finally, it is concluded that Al–Mg–Sc–Zr powder is suitable for reuse in the studied number of build cycles, if proper powder sieving and powder rejuvenation steps are included to preserve the required powder properties without detrimental effects on the repeatability and microstructural/mechanical properties of the manufactured LPBF parts.

CRediT authorship contribution statement

Laura Cordova: Conceptualisation, Methodology, Investigation, Writing - original draft. **Ton Bor**: Methodology, Supervision, Writing - review & editing. **Marc de Smit**: Resources, Investigation, Writing - review & editing. **Simone Carmignato**: Resources, Investigation, Writing - review & editing. **Mónica Campos**: Resources, Investigation, Writing - review & editing. **Tiedo Tinga**: Methodology, Supervision, Writing - review & editing, Funding acquisition.

Declaration of Competing Interest

The authors declare that they have no known competing financial interests or personal relationships that could have appeared to influence the work reported in this paper.

Acknowledgements

This research has been supported by the Dutch Research Council under project number 438-13-207, named "Sustainability Impact of New Technology on After sales Service supply chains (SINTAS)". The authors are grateful to Tim Hattenberg from the Netherlands Aerospace Centre (NLR), Eric Macía Rodríguez from the University Carlos III of Madrid, Sikander Naseem and Nachiket Deshmane from the University of Twente for their contribution to this paper.

References

[1] I. Gibson, D.W. Rosen, B. Stucker, Additive Manufacturing Technologies, Springer, New York, Heidelberg, Dordrecht, London, 2010.
[2] N.T. Aboulkhair, I. Maskery, C. Tuck, I. Ashcroft, N.M. Everitt, Improving the fatigue behaviour of a selectively laser melted aluminium alloy: influence of heat treatment and surface quality, Mater. Des. 104 (2016) 174–182.
[3] K.N. Amato, S.M. Gaytan, L.E. Murr, E. Martinez, P.W. Shindo, J. Hernandez, S. Collins, F. Medina, Microstructures and mechanical behavior of Inconel 718 fabricated by selective laser melting, Acta Mater. 60 (2012) 2229–2239.
[4] T.M. Mower, M.J. Long, Mechanical behavior of additive manufactured, powder-bed laser-fused materials, Mater. Sci. Eng. A 651 (2016) 198–213.
[5] L.C. Ardila, F. Garciandia, J.B. González-Díaz, P. Álvarez, A. Echeverria, M. M. Petite, R. Deffley, J. Ochoa, Effect of IN718 recycled powder reuse on properties of parts manufactured by means of selective laser melting, Phys. Proc. 56 (2014) 99–107.
[6] L. Cordova, T. Bor, M. de Smit, M. Campos, T. Tinga, Measuring the spreadability of pre-treated and moisturized powders for laser powder bed fusion, Addit. Manuf. 32 (2020), 101082.
[7] A.N.D. Gasper, B. Szost, X. Wang, D. Johns, S. Sharma, A.T. Clare, I.A. Ashcroft, Spatter and oxide formation in laser powder bed fusion of Inconel 718, Addit. Manuf. 24 (2018) 446–456.
[8] A.N.D. Gasper, D. Hickman, I. Ashcroft, S. Sharma, X. Wang, B. Szost, D. Johns, A. T. Clare, Oxide and spatter powder formation during laser powder bed fusion of Hastelloy X, Powder Technol. 354 (2019) 333–337.
[9] W. Nan, M. Pasha, T. Bonakdar, A. Lopez, U. Zafar, S. Nadimi, M. Ghadiri, Jamming during particle spreading in additive manufacturing, Powder Technol. 338 (2018) 253–262.
[10] O.A. Quintana, J. Alvarez, R. McMillan, W. Tong, C. Tomonto, Effects of reusing Ti-6Al-4V powder in a selective laser melting additive system operated in an industrial setting, JOM 70 (2018) 1863–1869.
[11] V. Seyda, N. Kaufmann, C. Emmelmann, Investigation of aging processes of Ti-6Al-4 V powder material in laser melting, Phys. Proc. 39 (2012) 425–431.
[12] H. Asgari, C. Baxter, K. Hosseinkhani, M. Mohammadi, On microstructure and mechanical properties of additively manufactured AlSi10Mg_200C using recycled powder, Mater. Sci. Eng. A 707 (2017) 148–158.
[13] A.H. Maamoun, M. Elbestawi, G.K. Dosbaeva, S.C. Veldhuis, Thermal post-processing of AlSi10Mg parts produced by selective laser melting using recycled powder, Addit. Manuf. 21 (2018) 234–247.
[14] F. Del Re, V. Contaldi, A. Astarita, B. Palumbo, A. Squillace, P. Corrado, P. Di Petta, Statistical approach for assessing the effect of powder reuse on the final quality of AlSi10Mg parts produced by laser powder bed fusion additive manufacturing, Int. J. Adv. Manuf. Technol. 97 (2018) 2231–2240.
[15] L. Cordova, M. Campos, T. Tinga, Revealing the effects of powder reuse for selective laser melting by powder characterization, JOM 71 (2019) 1062–1072.
[16] A.B. Spierings, K. Dawson, M. Voegtlin, F. Palm, P.J. Uggowitzer, Microstructure and mechanical properties of as-processed scandium-modified aluminium using selective laser melting, CIRP Ann. Manuf. Technol. 65 (2016) 213–216.
[17] A.B. Spierings, K. Dawson, K. Kern, F. Palm, K. Wegener, SLM-processed Sc- and Zr-modified Al-Mg alloy: mechanical properties and microstructural effects of heat treatment, Mater. Sci. Eng. A 701 (2017) 264–273.
[18] K. Schmidtke, F. Palm, A. Hawkins, C. Emmelmann, Process and mechanical properties: applicability of a scandium modified Al-alloy for laser additive manufacturing, Phys. Proc. 12 (2011) 369–374.
[19] F. Geiger, K. Kunze, T. Etter, Tailoring the texture of IN738LC processed by selective laser melting (SLM) by specific scanning strategies, Mater. Sci. Eng. A 661 (2016) 240–246.
[20] L. Cordova, E. Macia, M. Campos, T. Tinga, Mechanical properties of aluminum alloys produced by metal additive manufacturing, in: O.a.S.b. EPMA (Ed.), EUROPM2018 – Congress & Exhibition, Bilbao, 2018.
[21] J.P. Best, X. Maeder, J. Michler, A.B. Spierings, Mechanical anisotropy investigated in the complex SLM-processed Sc- and Zr-modified Al–Mg alloy microstructure, Adv. Eng. Mater. 21 (2018).
[22] ASTM E8/E8M − 15a, Standard Test Methods for Tension Testing of Metallic Materials, ASTM International, West Conshohocken, 2015.
[23] D. Lecompte, A. Smits, S. Bossuyt, H. Sol, J. Vantomme, D. Van Hemelrijck, A. M. Habraken, Quality assessment of speckle patterns for digital image correlation, Opt. Lasers Eng. 44 (2006) 1132–1145.
[24] P. Hermanek, S. Carmignato, Porosity measurements by X-ray computed tomography: accuracy evaluation using a calibrated object, Precis. Eng. 49 (2017) 377–387.
[25] F. Zanini, S. Carmignato, Two-spheres method for evaluating the metrological structural resolution in dimensional computed tomography, Meas. Sci. Technol. 28 (2017), 114002.
[26] P. Hermanek, F. Zanini, S. Carmignato, Traceable porosity measurements in industrial components using X-ray computed tomography, J. Manuf. Sci. Eng. 141 (2019).
[27] A.B. Spierings, K. Dawson, T. Heeling, P.J. Uggowitzer, R. Schäublin, F. Palm, K. Wegener, Microstructural features of Sc- and Zr-modified Al-Mg alloys processed by selective laser melting, Mater. Des. 115 (2017) 52–63.
[28] C. Weingarten, D. Buchbinder, N. Pirch, W. Meiners, K. Wissenbach, R. Poprawe, Formation and reduction of hydrogen porosity during selective laser melting of AlSi10Mg, J. Mater. Process. Technol. 221 (2015) 112–120.
[29] A.S. Bader, W. Faschinger, C. Schumacher, J. Geurts, L.W. Molenkamp, R.B. Neder, G. Karczewski, Real-time in situ X-ray diffraction as a method to control epitaxial growth, Appl. Phys. Lett. 82 (2003) 4684–4686.
[30] D.C.S. Grazulis, R.T. Downs, A.T. Yokochi, M. Quirós, L. Lutterotti, E. Manakova, J. Butkus, P. Moeck, A. Le Bail, Crystallography open database – an open-access collection of crystal structures, J. Appl. Crystallogr. 42 (2009) 726–729.
[31] R. Li, M. Wang, T. Yuan, B. Song, C. Chen, K. Zhou, P. Cao, Selective laser melting of a novel Sc and Zr modified Al-6.2 Mg alloy: processing, microstructure, and properties, Powder Technol. 319 (2017) 117–128.
[32] H. Zhang, D. Gu, J. Yang, D. Dai, T. Zhao, C. Hong, A. Gasser, R. Poprawe, Selective laser melting of rare earth element Sc modified aluminum alloy: thermodynamics of precipitation behavior and its influence on mechanical properties, Addit. Manuf. 23 (2018) 1–12.
[33] R. Li, H. Chen, H. Zhu, M. Wang, C. Chen, T. Yuan, Effect of aging treatment on the microstructure and mechanical properties of Al-3.02Mg-0.2Sc-0.1Zr alloy printed by selective laser melting, Mater. Des. 168 (2019), 107668.
[34] A.B. Spierings, K. Dawson, P.J. Uggowitzer, K. Wegener, Influence of SLM scan-speed on microstructure, precipitation of Al3Sc particles and mechanical properties in Sc- and Zr-modified Al-Mg alloys, Mater. Des. 140 (2018) 134–143.
[35] B. Van Hooreweder, D. Moens, R. Boonen, J.-P. Kruth, P. Sas, Analysis of fracture toughness and crack propagation of Ti6Al4V produced by selective laser melting, Adv. Eng. Mater. 14 (2012) 92–97.
[36] M.Y. Shaheen, A.R. Thornton, S. Luding, T. Weinhart, Discrete particle simulation of the spreading process in additive manufacturing, in: Proceedings of the 8th International Conference on Discrete Element Methods (DEM8), The Netherlands, 2019.
[37] D. Wang, S. Wu, F. Fu, S. Mai, Y. Yang, Y. Liu, C. Song, Mechanisms and characteristics of spatter generation in SLM processing and its effect on the properties, Mater. Des. 117 (2017) 121–130.
[38] Y. Liu, Y. Yang, S. Mai, D. Wang, C. Song, Investigation into spatter behavior during selective laser melting of AISI 316L stainless steel powder, Mater. Des. 87 (2015) 797–806.
[39] A.B. Anwar, Q.-C. Pham, Study of the spatter distribution on the powder bed during selective laser melting, Addit. Manuf. 22 (2018) 86–97.
[40] S. Tammas-Williams, P.J. Withers, I. Todd, P.B. Prangnell, The influence of porosity on fatigue crack initiation in additively manufactured titanium components, Sci. Rep. 7 (2017) 7308.
[41] N.T. Aboulkhair, N.M. Everitt, I. Ashcroft, C. Tuck, Reducing porosity in AlSi10Mg parts processed by selective laser melting, Addit. Manuf. 1–4 (2014) 77–86.
[42] S. Dietrich, M. Wunderer, A. Huissel, M.F. Zaeh, A. New, Approach for a flexible powder production for additive manufacturing, Proc. Manuf. 6 (2016) 88–95.
[43] C. Panwisawas, B. Perumal, R.M. Ward, N. Turner, R.P. Turner, J.W. Brooks, H. C. Basoalto, Keyhole formation and thermal fluid flow-induced porosity during laser fusion welding in titanium alloys: experimental and modelling, Acta Mater. 126 (2017) 251–263.
[44] A.B. Spierings, D. Bourell, N. Herres, G. Levy, Influence of the particle size distribution on surface quality and mechanical properties in AM steel parts, Rapid Prototyp. J. 17 (2011) 195–202.
[45] R.W. Hertzberg. Deformation and Fracture Mechanics of Engineering Materials, Fourth ed., John Wiley and Sons, Inc., Hoboken, NJ, 1996.